# CHAPTER IV

RESULTS AND DISCUSSION

4.1 Homoionic Clays

Homoionic hectorite and bentonite were prepared by purification and ion exchange method. In the purification process, quartz and other impurities were removed from bentonite by centrifugal technique. Quartz is the major component in rocks and minerals. It has low surface area and acidic site, which interrupts the analysis of clays. The Na ion is preferred to intercalate between the clay layers in order to obtain homoionic clays. The resulting products are white powder solid as the starting materials.

4.1.1 Purification of Bentonite

XRD patterns of raw material bentonite and purified bentonites collected from different centrifugal speeds are shown in Figure 4.1. All samples show the characteristic peaks of bentonite at 2-theta range of 7, 19 and 35 degree. At the centrifugal speed of 2000 rpm and lower, the 2-theta peak at 26.5 degree which was assigned to quartz (SiO_2) phase exists in the solid, suggesting free silica remains as an impurity on bentonite samples. The quartz peak disappeared in purified bentonite collected from the centrifugal speed of 4000 rpm, suggesting free silica was removed from raw material bentonite. Table 4.1 summarizes the d_{001} spacing of all samples during purification process. All collected samples from different centrifugal speeds show the d_{001} spacing in the range of 10 to 11 Å. The d_{001} peak of purified bentonites slightly shifts from raw material bentonite; however, their XRD patterns still show the characteristic peaks of bentonite. Therefore, purified bentonite obtained from the centrifugal speed of 4000 rpm, which

impurities particles were mostly removed at the centrifugal speed of 2000 rpm, is chosen as starting bentonite clay.
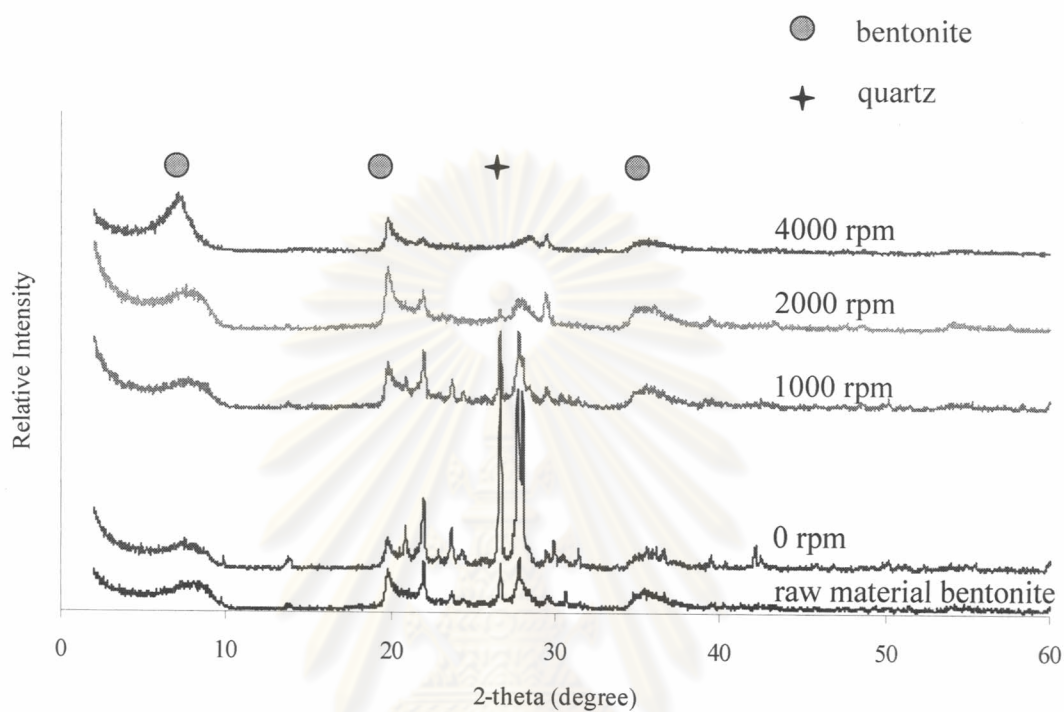
Figure 4.1 XRD patterns of raw material bentonite and purified bentonites collected from different centrifugal speeds.

Table 4.1 The d_{001} spacing of different centrifugal parts of bentonite

| Samples	d_{001}(Å)
Raw material bentonite	10.49
Particles collected at 0 rpm	11.07
Particles collected at 1000 rpm	10.74
Particles collected at 2000 rpm	10.82
Particles collected at 4000 rpm	11.96

4.1.2 The Effect of Na Sources and Concentrations

Hectorite

The relationship between the d_{001} spacing of hectorites and the number of Na-exchange is shown in Figure 4.2. It has clearly seen that the d_{001} spacings of Na-clays are higher than of the untreated one, which suggests Na ions intercalate between the clay layers. When the concentration of NaCl solution increases from 2M to 5M, the d_{001} spacing increases and becomes quite stable around 14 Å after ion exchange with 5M NaCl for four times. When the sodium sources between NaCl and NaOH were compared, it is found that the d_{001} spacing of hectorite treated with NaOH is higher than that treated with NaCl as shown in Table A-1. Figure 4.3 shows XRD patterns of hectorites treated with 5M NaOH. The clay characteristic peaks remain in all XRD patterns but changing to lower value of 2-theta, suggesting that Na ions intercalate into the clay layers and NaOH does not destroy the clay structure. The d_{001} spacings are quite stable around 15 Å when hectorite is treated more than four times. Therefore, hectorite treated with 5M NaOH for five times was chosen as a starting homoionic clay, which is named Na-Hectorite.
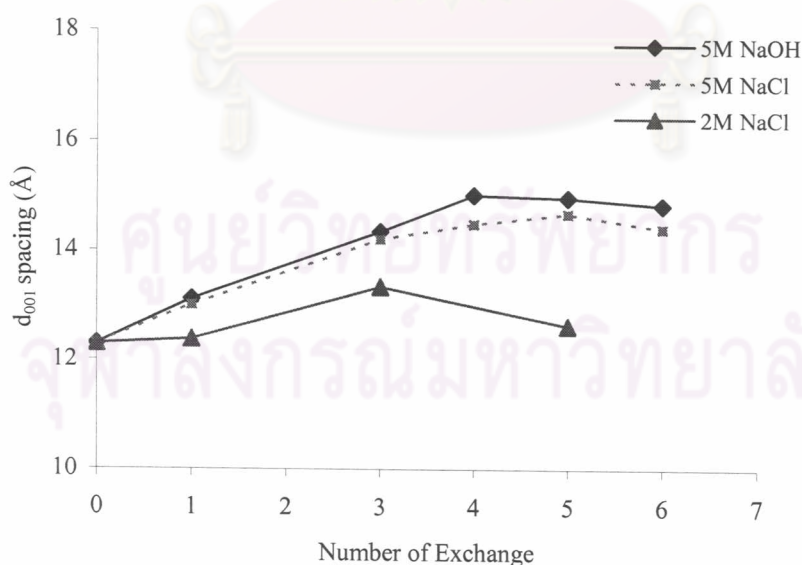

Figure 4.2 The relationship between the d_{001} spacings of hectorite and the number of Na exchange.
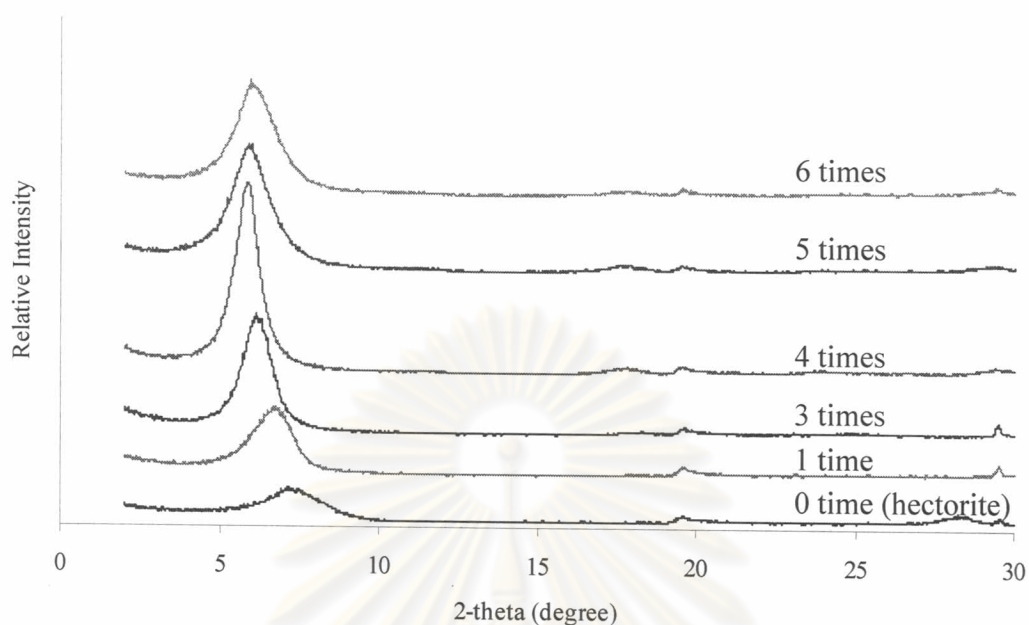
Figure 4.3   XRD patterns of hectorite treated with 5M NaOH.

Bentonite

Purified bentonite collected from the centrifugal speed of 4000 rpm, which impurities were removed at the centrifugal speed of 2000 rpm, was also treated with 5M NaOH. The XRD patterns of bentonite treated with 5M NaOH are shown in Figure 4.4 and the d_{001} spacing are summarized in Table 4.2. From XRD, the 2-theta value of bentonite treated with 5M NaOH is lower than untreated one suggesting Na ions intercalate into the clay layers and NaOH does not destroy the clay structure. The d_{001} spacing of Na-Betonite was quite stable when bentonite was treated since three times. Bentonite, treated with 5M NaOH three times, is selected as a starting homoionic clay, which is named Na-Bentonite.
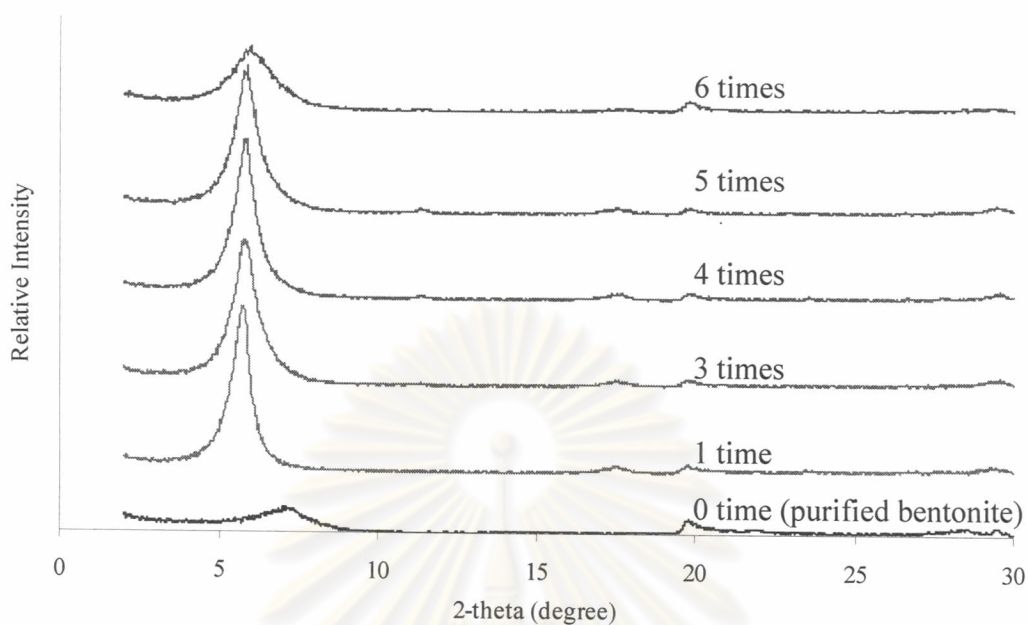
Figure 4.4   XRD patterns of purified bentonite treated with 5M NaOH.

**Table 4.2**   The d_{001} spacing of bentonite treated with 5M NaOH

Number of exchange	$d_{001}(\text{Å})$
Purified bentonite	11.96
1	15.22
3	14.91
4	14.81
5	14.81
6	14.42

4.2 The Characterization of Fe-pillared and Ga-doped Fe-pillared Clays

Fe-pillared and Ga-doped Fe-pillared clays were successfully synthesized. The obtained products are deep-red solids. The XRD patterns of all samples are shown in Figures 4.5 to 4.9. The shift of d_{001} reflection peak of clays was observed in all calcined samples. The synthesized method was successfully reproduced.

4.2.1 Intercalation of Fe-precursor into Clay Layer

XRD patterns of hectorite and Fe_{10}-intercalated hectorite (as-HFe_{10}) are shown in Figure 4.5. The d_{001} reflection peak of as-HFe_{10} was shifted from the 2-theta of 7 degree to 6.48 degree. The d_{001} spacing, which calculated from 2-theta value of as-HFe10, is higher than pure hectorite. The result can be described by intercalation of iron precursor which is larger than hydrated Na ion.
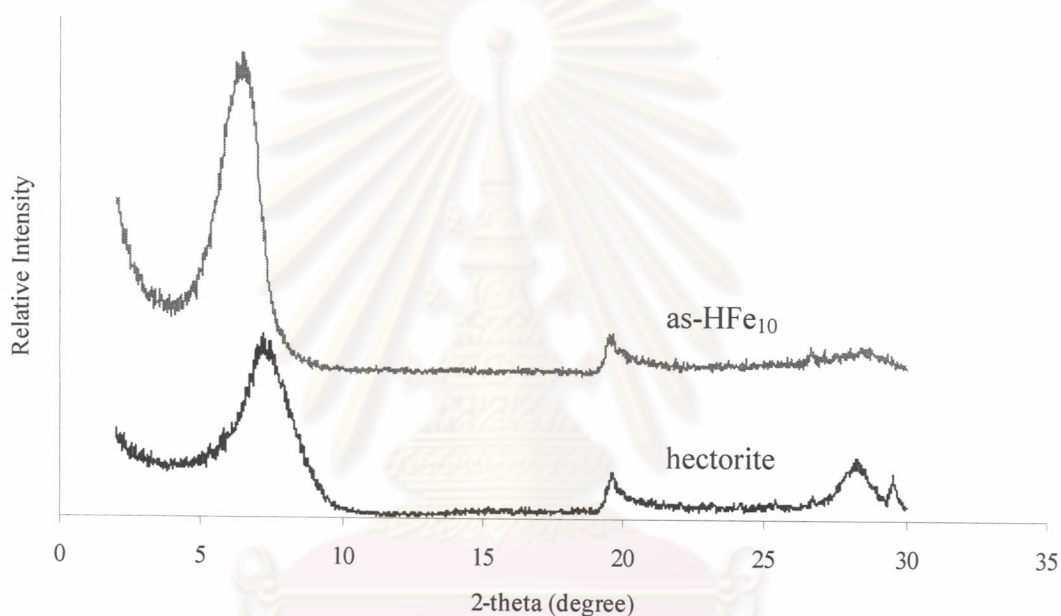

Figure 4.5   XRD patterns of hectorite and as-HFe_{10}.

4.2.2 Effect of Calcine Temperature

In order to find an optimal temperature for transformation of iron precursor to iron oxide in pillared clay, as-HFe_{10} was calcined between 300 and 600°C. Figure 4.6 shows XRD patterns of HFe_{10} at various temperatures. It has been seen that all HFe_{10}s show characteristic peak of d_{001} without destruction of clay structure and the d_{001} spacing decreases with increasing calcined temperature as shown in Table 4.3. Since 400°C, the d_{001} spacing dropped to around 9.6 Å and it remains constant when the calcine temperature was higher than 400°C. In this work, Fe-pillared clay with higher d_{001}

spacing is preferred because the organic reactants for catalytic reactions can be intercalated in pore site. At this point, the appropriate calcine temperature at $300^{\circ}C$ is chosen for this study.
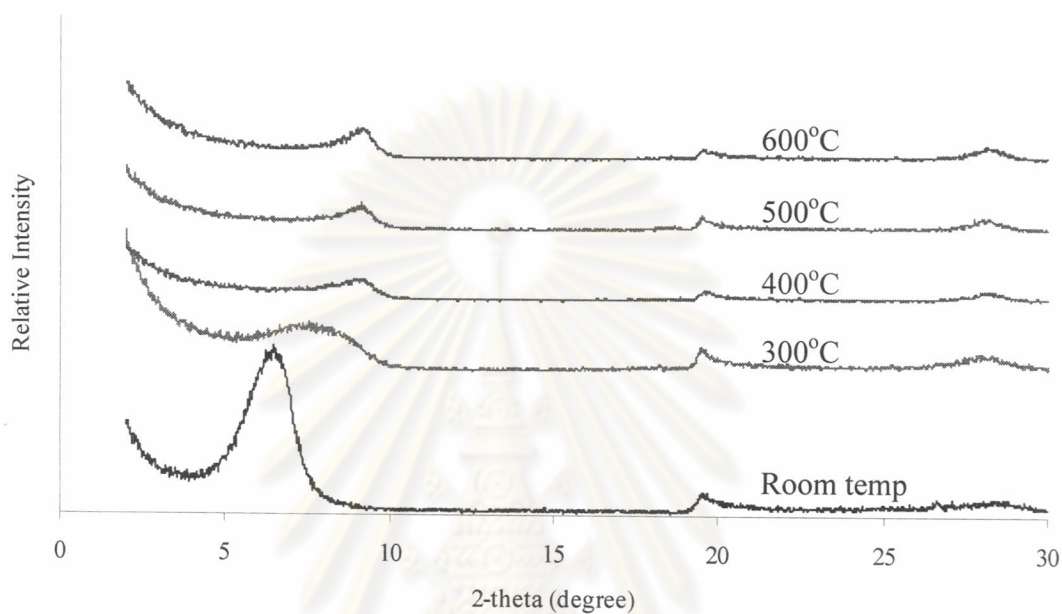
Figure 4.6   XRD patterns of HFe$_{10}$ at various calcined temperatures.

Table 4.3   The d$_{001}$ spacing of HFe$_{10}$ at various calcined temperatures

| Temperature (^{o}C)	d$_{001}$(Å)
Room	13.62
300	11.87
400	9.68
500	9.67
600	9.61

4.2.3 Effect of Iron Loading

In order to investigate effect of iron loading in pillaring agent on structure of catalyst, the amount of Fe in pillaring agent was varied between 0.5 to 240 meq per gram of clay and all as-synthesized products were calcined at $300^{\circ}C$ for 5 h. After calcination, the d_{001} spacing of all Fe-pillared hectorite differs from as-synthesized and calcined hectorite as shown in Table 4.4. It can be explained that water molecules which is absorbed between clay layers were removed and precursors were converted to iron oxide at calcine condition. From the difference in d_{001} spacing, the Fe-precursors are claimed to occupy in the interlayer[28,42]. This conclusion is supported by the data of AAS and N_2 adsorption-desorption isotherm as described in 4.2.5 and 4.2.7, respectively.

Table 4.4 The d_{001} spacing of Fe-pillared clays

| Samples	$d_{001}(\text{Å})$
Calcined hectorite	11.62
$HFe_{0.5}$	14.45
HFe_1	14.45
HFe_5	10.69
HFe_{10}	11.87
HFe_{20}	11.17
HFe_{240}	9.96
$HFe_{10}Ga_1$	10.42
$HFe_{10}Ga_1I$	10.53
Calcined bentonite	11.35
BFe_5	9.81
BFe_{10}	9.75
BFe_{20}	9.68
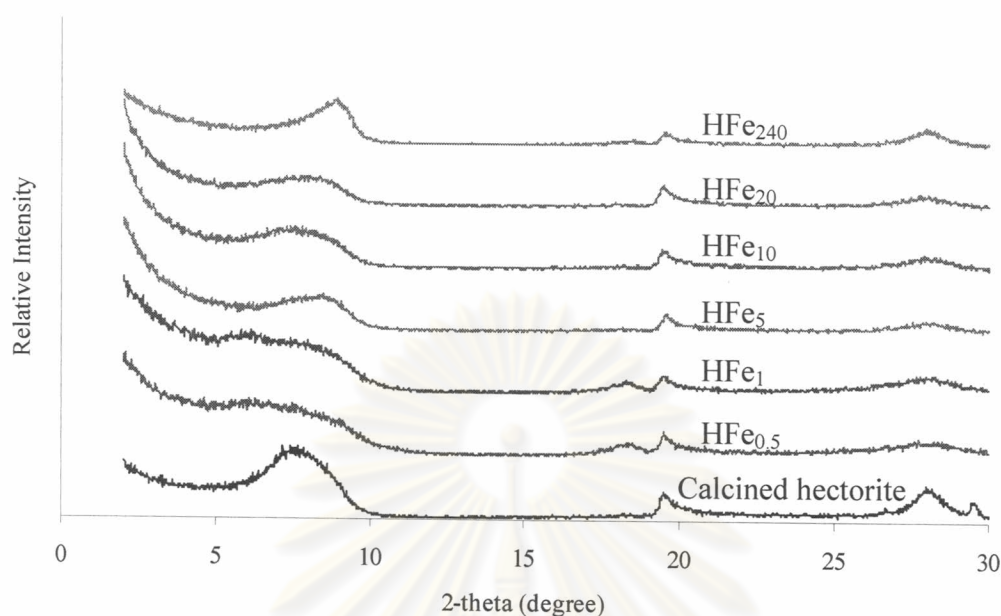
Figure 4.7   XRD patterns of calcined hectorite and Fe-pillared hectorites with various iron contents.

The d_{001} spacing of Fe-pillared hectorites depends on the amount of iron in pillaring agent. $HFe_{0.5}$ and HFe_1 show peak at 2-theta of 6.12 with a shoulder at 8.42 degree indicating that Fe-precursors do not intercalate in all clay layers[43]. The low d_{001} spacing is observed in HFe_{240} which due to the intercalation of small Fe-precursor cluster.

Ga-doped Fe_{10}-pillared hectorites were synthesized by two methods *i.e.* direct intercalation ($HFe_{10}Ga_1$) and impregnation ($HFe_{10}Ga_1I$). The d_{001} spacings of $HFe_{10}Ga_1$ and $HFe_{10}Ga_1I$ are summarized in Table 4.4. The results show that the d_{001} spacings of $HFe_{10}Ga_1$ and $HFe_{10}Ga_1I$ are slightly different from that of HFe_{10}. Their XRD patterns compared with HFe_{10} are shown in Figure 4.8. The characteristic peaks of clay are observed in both Ga-doped Fe_{10}-pillared hectorites, indicating that gallium does not affect the clay structure.
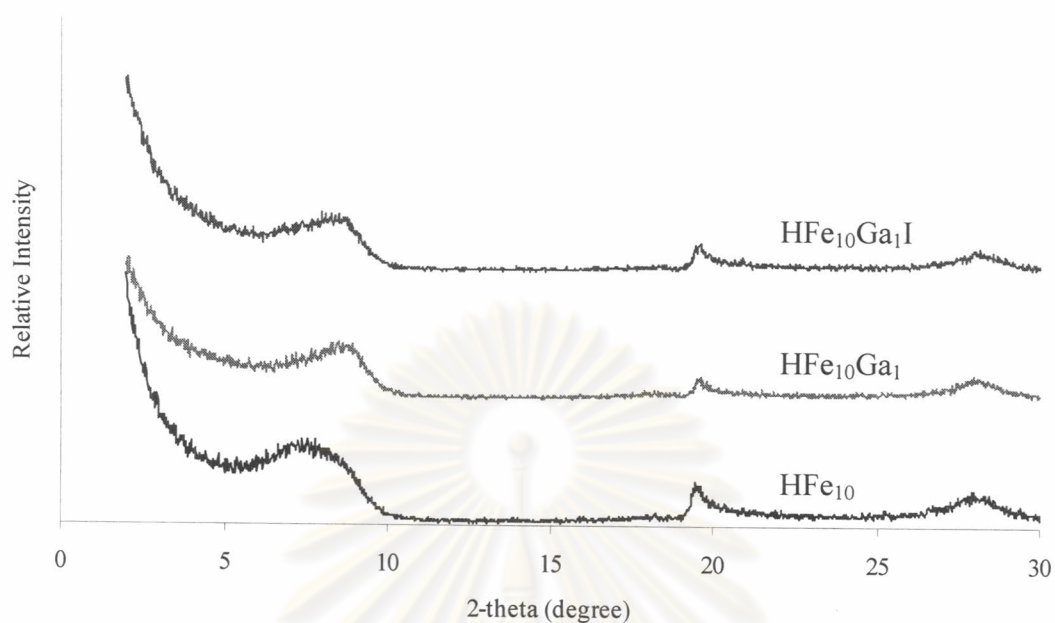
Figure 4.8   XRD patterns of HFe_{10} and Ga-doped Fe-pillared hectorites.
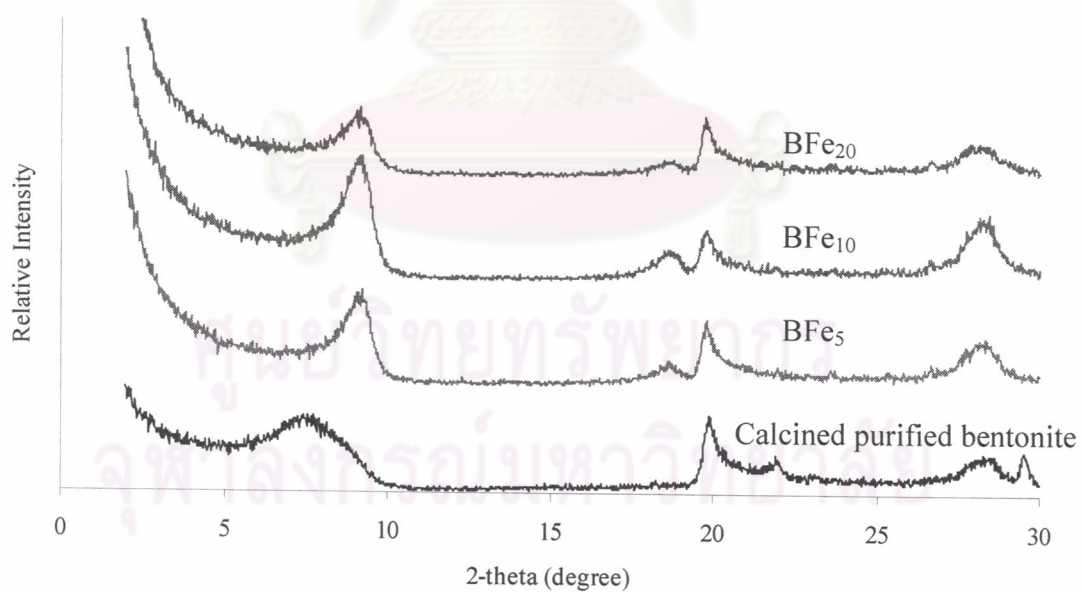
Figure 4.9   XRD patterns of calcined purified bentonite and Fe-pillared bentonite with various iron contents.

For the bentonite support, Table 4.4 shows d_{001} spacing of calcined purified bentonite and Fe-pillared bentonite. The d_{001} reflection peak of Fe-pillared bentonites (BFe_x) was also shifted to lower value compared with calcined purified bentonite and it is quite constant around 10Å as shown in Figure 4.9. This result can be described earlier in Fe-pillared hectorite.

4.2.4 Scanning Electron Microscope

The surface morphology of hectorite and Fe-pillared hectorite were investigated using SEM. SEM images of hectorite and HFe_{10} are shown in Figure 4.10. Hectorite shows the layer structure. It has been seen that clay-layered structure is observed in HFe_{10} indicating that HFe_{10} still have layer structure.

(a)   (b)

Figure 4.10   SEM images of hectorite (a) and HFe_{10} (b).

To investigate distribution of metal on Fe-pillared clay, elemental ion mapping of HFe_{10} was performed and photographs are shown in Figure 4.11. It can be explained that Fe ion is homogeneous distribution in the clay structure. Besides, no aggregation of Fe_2O_3 was observed on the clay surface suggesting that Fe precursors intercalate in the clay layer as Fe_2O_3 after calcination.
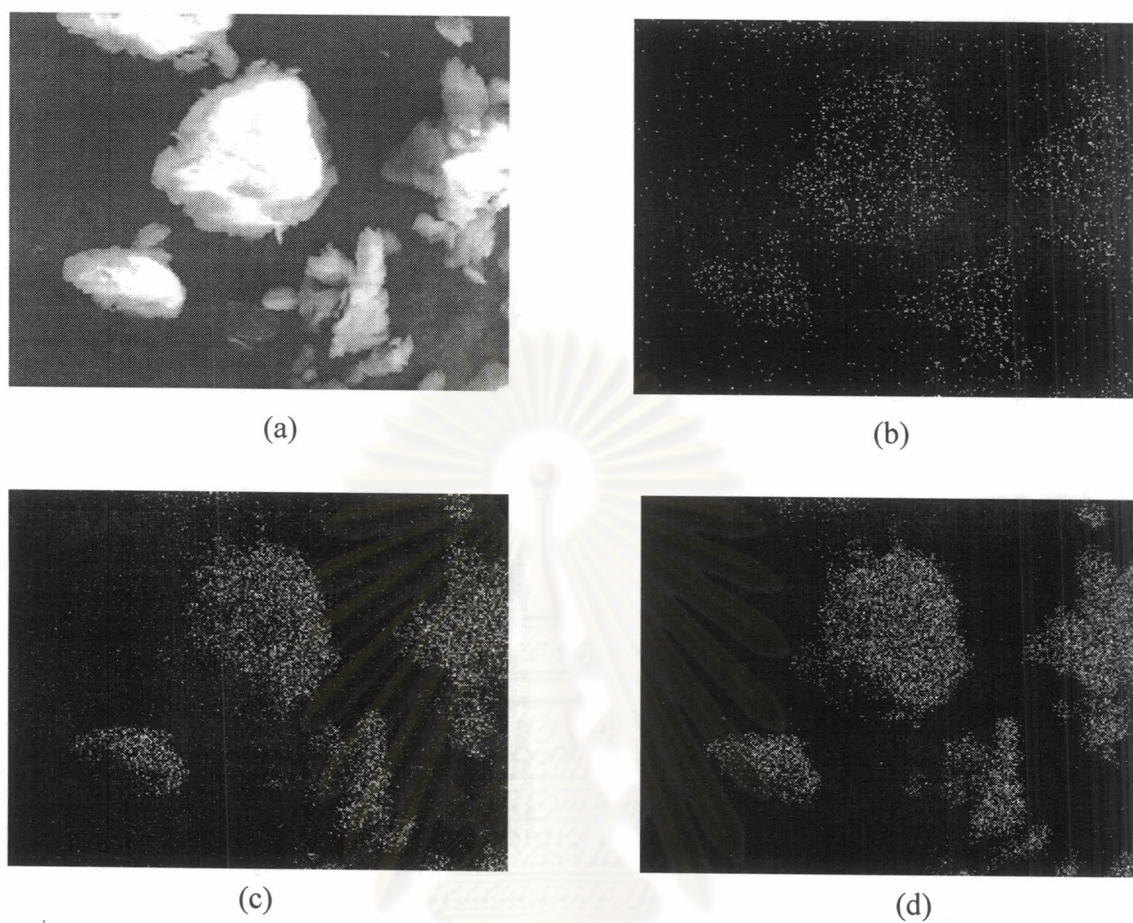
Figure 4.11 SEM of HFe_{10} (a), and its elemental ion mapping images: Fe ion (b), Mg ion (c) and Si ion (d).

4.2.5 Fourier Transform Infrared Spectroscopy (FT-IR)

The FT-IR spectra of hectorite and Fe-pillared hectorites with Fe content up to 240 meq per gram of hectorite are shown in Figure 4.12. It has been reported that Si-O bond stretching vibration shows FT-IR band at ~1000 cm^{-1} with a shoulder at 1200 cm^{-1}. The bands at 1630 and 3400 cm^{-1} belong to the O-H bending and stretching of water, respectively[44]. The absorption bands at 1450 and 3600 cm^{-1} are due to the O-H bending and the stretching of hydroxyl groups in clay sheet, respectively[45]. The band at 980 cm^{-1} is due to the Si-OH bond. The Si-O bonds in framework structure[46] are shown at 800 and 470 cm^{-1}.

All Fe-pillared hectorites (HFe$_x$) with various iron contents still show the absorption bands about 800 and 470 cm^{-1} indicating that the Si-O bonds in the framework structure remain. Therefore, the intercalation of Fe precursor does not destroy the clay-layer structure. Due to the formation of Si-O-Fe bond, the Si-O band was shift from 1003 to 1022 cm^{-1} with an increase in iron contents, whereas hectorite shows the Si-O band at 999 cm^{-1}[45]. The absorption band at 1450 cm^{-1} is not observed in all Fe-pillared hectorite because the proton of the O-H bending of hydroxyl groups in clay sheet is removed by OH ion in the exchangeable process.
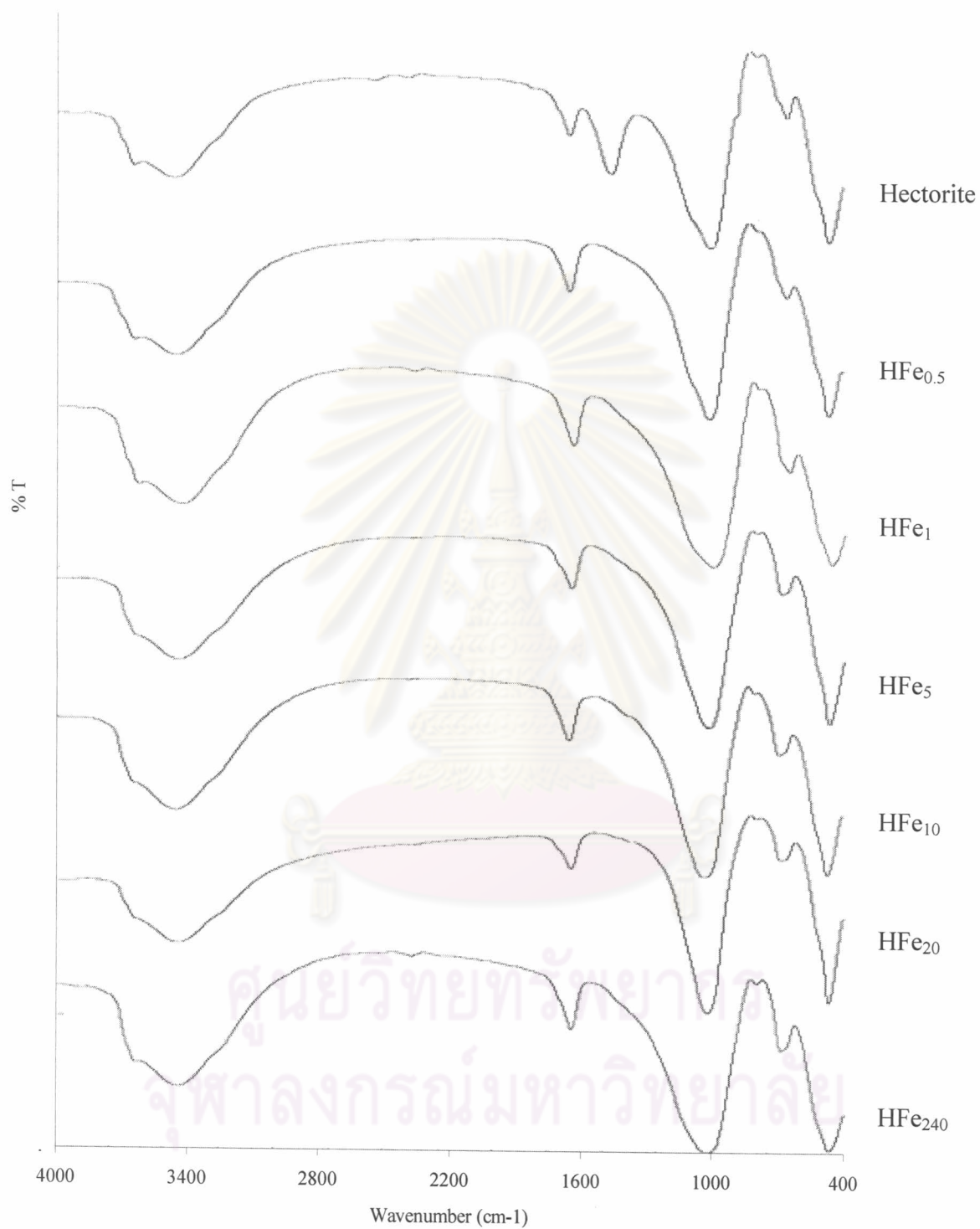
Figure 4.12 FT-IR spectra of hectorite (HFe_0) and Fe-pillared hectorites (HFe_x).

4.2.6 Determination of Iron and Gallium Contents

The iron contents in calcined samples were analyzed by AAS technique. Table 4.5 reports the iron contents in form of Fe_2O_3. The iron contents in calcined samples are higher than pure clays. For Fe-pillared hectorites, the iron contents increase with increasing amount of iron in pillaring agent. The iron contents are quite constant when iron in pillaring agent is raised from 5 to 20 meq per gram of clay. It may be explained by the limitation of cation exchange capacity (CEC) in hectorite. The smectite clay, hectorite and bentonite has CEC about 100 meq per gram[31]. If the iron in pillaring agent is higher than 10 meq, it can be difficult to intercalate into the clay layer. Because iron can be reduced by O_2 in air, it can coaggulate to iron oxide cluster which does not intercalate into clay layer[47]. It is also possible that due to the character of Fe-precursors, diffusion between the clay layer is slow and intercalation is limited which leads to deposition of Fe-species on the external surface[47]. This explanation can be seen on the HFe_{240} whose the iron content was droped to 12.30%.

For Fe-pillared bentonites, iron content was in the same trend as Fe-pillared hectorite. It can be concluded that the difference of metal in octahedral clay framework does not affect the intercalation of iron pillaring precursors. Bentonite is composed of Al_2O_3 in octahedral sheet whereas hectorite is MgO_2.

Table 4.5   The iron contents in clays and Fe-pillared clays

Samples	% Fe_2O_3
Hectorite	1.60
$HFe_{0.5}$	4.81
HFe_1	7.99
HFe_5	21.83
HFe_{10}	24.61
HFe_{20}	22.36
HFe_{240}	12.30

Table 4.5 (continued)   The iron contents in clays and Fe-pillared clays

Samples	% Fe_2O_3
Bentonite	6.61
BFe_5	29.69
BFe_{10}	30.19
BFe_{20}	31.41

The amount of gallium in Ga-doped HFe_{10} was analyzed by ICP and data in form of Ga_2O_3 are summarized in Table 4.6. $HFe_{10}Ga_1I$ exhibits higher gallium content than $HFe_{10}Ga_1$ because $HFe_{10}Ga_1$ was synthesized by co-ions intercalation method. Thus, the amount of gallium cooperated in the structure may be less than the direct impregnation.

Table 4.6   The iron and gallium contents in hectorite and Ga-doped Fe-pillared hectorite

Samples	% Fe_2O_3	% Ga_2O_3
Hectorite	1.60	0.03
$HFe_{10}Ga_1$	19.03	1.19
$HFe_{10}Ga_1I$	19.24	3.39

4.2.7 Nitrogen Adsorption-Desorption

The BET specific surface area and pore diameter of Fe-pillared clays (HFe_x and BFe_x) are shown in Table 4.7. The Nitrogen adsorption-desorption isotherm and pore size distribution of clays and Fe-pillared clays are shown in Figures A-1 to A-11. The reversible distorted type IV isotherms are observed for all Fe-pillared clays indicating that Fe_2O_3 in calcined samples converted clay-layered structure (2D structure) to micro-mesoporous structure (3D structure). Therefore, the BET specific surface areas of Fe-pillared clays were higher than pure clays. The BET specific surface area of Fe-pillared clays depends on iron content. As iron contents in calcined samples are increased, the BET specific surface areas are also increased and it becomes constant when the iron content reaches 10 meq. This result correlates with XRD pattern and the

data of iron content described earlier in 4.2.3 and 4.2.6, respectively. Until the iron content was 240 meq, the BET specific surface area was dropped to 105 m^2/g because HFe_{240} had lower iron content and d_{001} spacing value than the others as described earlier in 4.2.3 and 4.2.6.

Table 4.7 The BET specific surface area and pore diameter of Fe-pillared clays

Samples	BET specific surface area (m^2/g)	BJH pore diameter (Å)
Hectorite	74.82	-
$HFe_{0.5}$	81.79	38.12
HFe_1	109.00	38.22
HFe_5	145.18	38.16
HFe_{10}	176.08	38.17
HFe_{20}	175.14	38.08
HFe_{240}	105.92	38.08
Bentonite	71.06	-
BFe_5	187.60	38.17
BFe_{10}	153.63	38.20
BFe_{20}	160.76	38.13

The BET specific surface areas of Ga-doped Fe-pillared hectorites from two synthesized methods are compared with hectorite and HFe_{10} as shown in Table 4.8. $HFe_{10}Ga_1$ and $HFe_{10}Ga_1I$ show higher BET specific surface areas than hectorite but slightly lower comparing with HFe_{10}. Especially, for $HFe_{10}Ga_1I$, gallium deposited on the pore wall of HFe_{10} causing the BET specific surface area and pore diameter being reduced. However, Ga-doped Fe-pillared hectorites still show reversible distorted type IV isotherms which indicate that they have micro-mesoporous structure also.

Table 4.8 The BET specific surface area and pore diameter of hectorite, HFe_{10} and Ga-doped Fe-pillared hectorites

Samples	BET specific surface area (m^2/g)	BJH pore diameter (Å)
Hectorite	74.82	-
HFe_{10}	176.08	38.17
$HFe_{10}Ga_1$	162.23	38.03
$HFe_{10}Ga_1I$	163.76	37.63

4.3 Used Catalyst
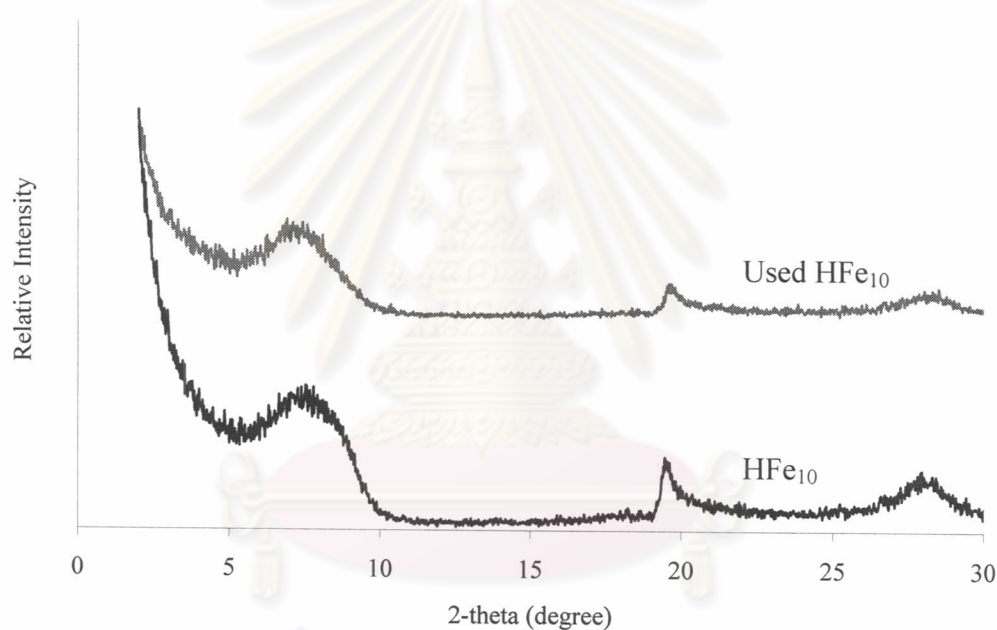
Figure 4.13 XRD patterns of HFe_{10} and used HFe_{10}.

XRD patterns of HFe_{10} and used HFe_{10} are shown in Figure 4.13. The results show that both samples have the same structure with d_{001} spacing of 11.86 Å, suggesting the structure of catalyst did not destroy after the reaction. Although the catalyst was recalcined at 300°C for 5h, the structure of clay catalyst was still remained. However, the BET surface area of used catalyst decreases as shown in Table 4.9. It may be due to blocking of organic compound in catalyst pore.

Table 4.9   The BET specific surface area and pore diameter of HFe_{10} and used HFe_{10}

Catalysts	BET specific surface area (m^2/g)	BJH pore diameter (Å)
HFe_{10}	176.08	38.17
used HFe_{10}	116.94	38.36

4.4 Catalytic Activity of Fe-pillared and Ga-doped Fe-pillared Clays in Alkylation Reaction

Alkylation of benzene with 1-dodecene to produce phenyldodecane was selected for testing the catalytic activity of Fe-pillared clays and gallium-doped Fe-pillared clay. The reaction temperature and time were varied to find the optimal condition.

Phenyldodecane has five isomers, *i.e.* 2-, 3- ,4-, 5-, 6-phenyldodecanes, as shown in Figure A-14[48-49]. The isomer products were identified by GC-MS and the mass spectra are shown in Figures A-15 to A-19. The parent peak observed at m/z = 105 in Figure A-15 is assigned to the ion of 2-phenyldodecane. The parent peaks observed at m/z = 91 and 119 in Figure A-16 are assigned to the 3-phenyldodecane ion. The parent peaks observed at m/z = 91 and 133 in Figure A-17 are assigned to the 4-phenyldodecane ion. The parent peaks observed at m/z = 91 and 147 in Figure A-18 are assigned to the 5-phenyldodecane ion. The parents peak observed at m/z = 91, 105, 119, 161 and 175 in Figure A-19 are assigned to the 6-phenyldodecane ion.

In this research, phenyldodecane was focused as a main product. Therefore, the products occurred from isomerization of 1-dodecene *e.g.* 2-dodecene and 4-dodecene [48] were reported as the other products.

4.4.1 Effect of Temperature

HFe_{10} was used as a catalyst for obtaining the best reaction temperature. The catalytic activity of HFe_{10} is summarized in Table 4.10. At room temperature, the alkylation of benzene with 1-dodecene does not occur but with increasing temperature,

the conversion of 1-dodecene and the selectivity to phenyldodecane product increases. The selectivity to 2-phenyldodecane isomer also decreases from 58 to 49% when the reaction temperatures are raised to $150^{o}C$. Even though, there was no difference in the selectivity to phenyldodecane product and 2-phenyldodecane isomer after $100^{o}C$, conversion of 1-dodecene at $120^{o}C$ was slighly higher than others. Therefore, the reaction temperature at $120^{o}C$ was chosen for further investigation.

Table 4.10 Catalytic activity of HFe_{10} with various reaction temperatures

Temp. (^{o}C)	Time (min)	%C_{12} conversion	% Selectivity to		% Selectivity to phenyl isomer				
			Phenyldo-decane	Others	2-	3-	4-	5-	6-
R.T.	30	0	0	0	0	0	0	0	0
60	30	3.33	6.93	93.07	58.55	17.91	11.35	7.60	4.61
80	30	8.20	8.25	91.75	59.81	17.46	10.69	7.44	4.61
100	30	69.82	21.78	78.23	49.68	21.01	13.06	9.93	6.31
120	30	72.50	21.15	78.85	45.27	21.09	14.23	11.64	7.77
150	30	69.27	21.11	78.89	49.15	20.78	13.25	10.40	6.44

4.4.2 Effect of Reaction Time

HFe_{10} is also used as catalyst for obtaining the best reaction time. The results from Table 4.11 show that at $120^{o}C$, the conversion of 1-dodecene and the selectivity to phenyldodecane product increase with increasing reaction time. The highest conversions of 1-dodecene and the selectivity to phenyldodecane product were obtained when reaction time was expanded to 600 min. On the contrary, the selectivity to 2-phenyldodecane was decreased while other isomers were increased. Although the selectivity to phenyldodecane product was not different between the reaction time at 15 and 30 min, conversion of 1-dodecene at 30 min was higher than that at 15 min. Therefore, the optimal reaction time would be 30 min.

Table 4.11 Catalytic activity of HFe_{10} with various reaction times

Temp. (^{o}C)	Time (min)	%C_{12} conversion	% Selectivity to		% Selectivity to phenyl isomer				
			Phenyldo-decane	Others	2-	3-	4-	5-	6-
120	15	43.31	19.79	80.21	51.44	20.06	12.68	9.68	6.15
120	30	72.50	21.15	78.85	45.27	21.09	14.23	11.64	7.77
120	240	86.70	35.57	64.43	34.30	20.60	17.38	16.09	11.63
120	600	99.72	43.31	56.69	30.93	20.31	18.02	15.55	15.22

4.4.3 Effect of Iron Content

From the previous results, the optimal reaction condition was set at 120°C for 30 min and used for studying the effect of iron content in the reaction. The catalytic activity of Fe-pillared hectorites is compared with iron oxide (Fe_2O_3, hematite) and pure hectorite in Table 4.12. The alkylation of benzene with 1-dodecene does not occur without catalyst and Fe_2O_3 does not catalyze the reaction. For the Fe-pillared clays, the catalytic activity depends on iron contents. Conversions of 1-dodecene and selectivity to phenyldodecane product incresed with increasing iron content in the pillared clay and become decreased when the iron content in pillaring agent is too high. This result is in agreement with the BET specific surface area of catalyst being discussed earlier.

ศูนย์วิทยทรัพยากร
จุฬาลงกรณ์มหาวิทยาลัย

Table 4.12   Catalytic activity of hectorite, Fe_2O_3 and Fe-pillared hectorites

Catalysts	%C_{12} conversion	% Selectivity to		% Selectivity to phenyl isomer				
		Phenyldo-decane	Others	2-	3-	4-	5-	6-
No	0	0	0	0	0	0	0	0
Hectorite	7.74	1.60	98.40	61.90	17.62	9.27	6.98	4.23
Fe_2O_3	0	0	0	0	0	0	0	0
HFe_1	7.31	5.60	94.41	53.60	18.78	12.39	9.20	6.04
HFe_5	60.84	20.31	79.69	52.08	20.43	12.35	9.30	5.83
HFe_{10}	72.50	21.15	78.85	45.27	21.09	14.23	11.64	7.77
HFe_{20}	41.67	14.42	85.59	54.08	19.61	11.69	9.19	4.60
HFe_{240}	30.60	16.50	83.51	53.81	19.65	11.51	9.55	5.50

Fe-pillared bentonites (BFe_x) were also tested for the catalytic activity at 120° for 30 min. The activity of all BFe_xs are compared with purified bentonite and summarized in Table 4.13. The catalytic activity depends on iron contents. All BFe_xs show the conversion of 1-dodecene and the selectivity to phenyldodecane product as high as HFe_x. Moreover, 2-phenyl isomer is also prefered than other isomers. From the catalytic results of HFe_x and BFe_x, it can be concluded that type of clays (hectorite and bentonite) do not affect on the catalytic activity in this reaction.

Table 4.13   Catalytic activity of bentonite and Fe-pillared bentonites

Catalysts	%C_{12} conversion	% Selectivity to		% Selectivity to phenyl isomer				
		Phenyldo-decane	Others	2-	3-	4-	5-	6-
Bentonite	7.05	1.13	98.87	53.02	19.40	12.46	8.54	6.58
BFe_5	61.41	15.96	84.02	53.35	20.90	11.83	8.58	5.36
BFe_{10}	68.20	22.85	77.16	47.60	21.64	13.47	10.41	6.88
BFe_{20}	61.57	15.01	84.99	54.96	20.46	11.38	8.19	5.03

4.4.4 Effect of Gallium in Ga-Doped Fe-pillared Hectorite

The catalytic activity of Ga-doped Fe_{10}-pillared hectorites are shown in Table 4.14. Ga_2O_3 does not catalyze the akylation of benzene with 1-dodecene. The conversion of 1-dodecene was decreased from 72 to 44% when gallium was added to clay. This can be explained by the lower BET specific surface area of Ga-doped Fe_{10}-pillared hectorite. The Ga-doped Fe_{10}-pillared hectorite synthesized by direct intercalation shows lower conversion of 1-dodecene than those synthesized by impregnation. This might be due to the difference in gallium content in the catalyst. However, both catalysts mainly produce 2-phenyldodecane up to 55%.

Table 4.14 Catalytic activity of Ga-doped HFe_{10}

Catalysts	%C_{12} conversion	% Selectivity to		% Selectivity to phenyl isomer				
		Phenyldo-decane	Others	2-	3-	4-	5-	6-
HFe_{10}	72.50	21.15	78.85	45.27	21.09	14.23	11.64	7.77
Ga_2O_3	0	0	0	0	0	0	0	0
$HFe_{10}Ga_1$	44.02	17.11	82.89	57.80	19.23	10.37	7.89	4.71
$HFe_{10}Ga_1I$	59.05	24.56	75.44	55.61	19.90	11.33	8.34	4.83

4.4.5 Reused Catalyst

The reusing of catalyst was studied using HFe_{10}. Although the catalyst was recalcined at 300°C for 5h as the fresh catalyst, the lower BET surface area of used catalyst are observed (as shown in Table 4.9). The used catalyst not only exhibits lower converion of 1-dodecene, but the selectivity to phenyldodecane product are also decreased. Both catalysts prefers to produce 2-phenyldodecane isomer product than other isomers up to 45%.

Table 4.15   Catalytic activity of HFe_{10}

Cycle of reaction	%C_{12} conversion	% Selectivity to		% Selectivity to phenyl isomer				
		Phenyldo-decane	Others	2-	3-	4-	5-	6-
1	72.50	21.15	78.85	45.27	21.09	14.23	11.64	7.77
2	55.68	17.97	82.03	57.08	19.79	10.78	7.78	4.57